HHS Public Access

Author manuscript

Nature. Author manuscript; available in PMC 2011 August 17.

Published in final edited form as:

Nature. 2011 February 17; 470(7334): 353–358. doi:10.1038/nature09793.

Asymmetric Cell Divisions Promote Notch-Dependent Epidermal Differentiation

Scott E. Williams, **Slobodan Beronja**, **H. Amalia Pasolli**, and **Elaine Fuchs**[1]

Howard Hughes Medical Institute, Laboratory of Mammalian Cell Biology & Development, The Rockefeller University, New York, New York 10065, USA.

Summary

Stem and progenitor cells utilize asymmetric cell divisions to balance proliferation and differentiation. Evidence from lower eukaryotes shows that this process is regulated by proteins asymmetrically distributed at the cell cortex during mitosis: (1) Par3-Par6-aPKC, conferring polarity; (2) Gαi-LGN/AGS3-NuMA-p150^{glued}, governing spindle positioning. Here, we focus on developing mouse skin, where progenitors execute a switch from predominantly symmetric to asymmetric divisions concomitant with stratification. Using in vivo skin-specific lentiviral RNAi, we investigate spindle orientation regulation and provide direct evidence that LGN, Numa1 and Dctn1 are involved. In compromising asymmetric cell divisions, we uncover profound defects in stratification, differentiation and barrier formation, and implicate Notch signalling as an important effector. Our study demonstrates the efficacy of applying RNAi in vivo to mammalian systems, and the ease of uncovering complex genetic interactions, here to gain insights into how changes in spindle orientation are coupled to establishing proper tissue architecture during skin development.

Introduction

Asymmetric cell divisions (ACDs) are important regulators of stem cell and cancer biology.1 The genetic pathways underlying spindle orientation and ACDs have been best studied in *C. elegans* and *Drosophila*, where conserved sets of proteins are asymmetrically distributed at the cell cortex during mitosis: the Par complex—consisting of Bazooka(Par3), Par6 and atypical protein kinase C(aPKC)—functions as a master polarity determinant, while Gαi, Pins(LGN/AGS3), Mud(NuMA) and p150^{glued}(Dctn1), regulate spindle positioning.2,3 In *Drosophila* neuroblasts, Inscuteable links these complexes by binding to both Par3 and Pins.

[1]To whom correspondence should be addressed: Elaine Fuchs, Howard Hughes Medical Institute, Laboratory of Mammalian Cell Biology & Development, The Rockefeller University, 1230 York Avenue, Box 300, New York, NY, 10065, USA. Phone: 212-327-7953, Fax: 212-327-7954, fuchslb@rockefeller.edu.

Supplementary Information

Supplementary information includes 12 figures.

Author Contributions

S.E.W., E.F. and S.B. designed experiments. S.E.W. performed the experiments and analysed their raw data. H.A.P. conducted ultrastructural analyses. S.E.W. and S.B. performed lentiviral injections. S.E.W. and E.F. wrote the paper. All authors provided intellectual input, read and approved the manuscript.

Author Information

The authors declare no competing financial interests.

4–6 As neuroblasts progress through mitosis, Insc/Pins/Mud polarize and segregate into one daughter, retaining its progenitor status, while the other daughter inherits oppositely polarized proteins including the Notch inhibitor Numb, which promotes differentiation.2,3

ACDs have also been documented in vertebrates, including in mouse skin, where a shift from predominantly parallel/symmetric to perpendicular/asymmetric divisions occurs at embryonic day (E)14 coincident with stratification.7–9 Basal delamination has been implicated in the process, and although ACDs could be critical,10 direct functional evidence is lacking to support or refute a role for ACDs in promoting tissue growth and architecture for this or any other mammalian system.

As in lower eukaryotes, ACD components polarize in mitotic basal keratinocytes, forming an apical crescent of LGN and an interacting partner, NuMA.7,11–13 NuMA in turn binds microtubules and cytoplasmic dynein, partially colocalising with the $p150^{glued}$/Dctn1 dynein-dynactin component in cultured keratinocytes.7 LGN is thought to be recruited to the cell cortex through GPI-linked Gαi/Gαo, which binds LGN's C-terminal GoLoco motifs. Such interactions likely reorient the mitotic spindle through cortical capture of astral microtubules.14–18

To explore the physiological relevance of the LGN/NuMA/Dctn1 pathway, we devised a strategy to efficiently knockdown its constituents at a time during skin development when divisions become primarily asymmetric. Our method employs ultrasound-mediated delivery of high-titre lentivirus into amniotic space.19 Lentivirus selectively transduces the first cell layer it encounters, which shortly after gastrulation is single-layered epidermis. Avoiding tissue-specific promoters, we achieve efficient infection, stable integration and sustained epidermal expression of short-hairpin RNAs (shRNAs) at the requisite early developmental stage that permits analysis of their consequences to ACD.

Results

ACD components control spindle orientation

LGN regulates spindle orientation and promotes planar cell divisions in other systems,20–22 but is symmetrically inherited in each case. In developing skin, however, LGN remained apical even after cleavage furrow formation (Fig. 1a). LGN colocalised with NuMA and Gαi3 in mitotic basal cells, while Dctn1 localised to centrosomes and cell cortex, where it frequently polarized with apical enrichment at mitosis (Fig. 1b; Supplementary Fig. 1). Thus, not only are these divisions operationally defined as asymmetric, but in addition, ACD components appeared to partition selectively to the apical daughter.

To address whether *LGN*, *Numa1*, and *Dctn1* function in spindle orientation and skin biology, we first identified shRNAs23 that reduced (often >90%) target mRNA expression in cultured keratinocytes (Fig. 1c). To guard against potential off-target effects, and also generate allelic series, we selected multiple hairpins for each gene studied. To label transduced skin cells, we cloned shRNAs into lentiviral vectors harbouring a fluorescent reporter (*H2B-mRFP1*, *H2B-YFP*, *H2B-CFP*).

E9.5 embryos were transduced (70–95%) *in utero* with lentiviruses harbouring *LGN*, *Numa1*, *Dctn1* or control (non-targeting) *Scramble* shRNAs (Supplementary Fig. 2). Expression was propagated stably, as evidenced by strong RFP in differentiated/suprabasal progeny of infected basal cells. Fluorescence activated cell sorting (FACS) was used to quantify knockdown efficiencies and analyse cell cycle kinetics, mRNA, and protein expression. As shown for *LGN*, and with similar results for *Numa1* and *Dctn1*, maximal knockdown (~80% with *shLGN-1617*) was attained by stratification onset and maintained throughout development (Fig. 1d; Supplementary Fig. 1).

To explore whether LGN/NuMA/Dctn1 orient the spindle and promote ACDs, we knocked down each component and measured the division angle in late-stage mitotic H2B-RFP^{+} (transduced/knockdown) and H2B-RFP^{neg} (non-tranduced/control) basal cells. Quantifications were aided by co-labelling with the anaphase/telophase marker survivin (Fig. 1e–g). In E16.5 basal cells infected with *shScramble*-virus, ~36% of divisions were symmetric (within 20° of horizontal), while most were asymmetric (~46% perpendicular, ~18% oblique), a distribution identical to wild-type littermates. In contrast, basal cells transduced with *LGN*, *Numa1*, or *Dctn1 shRNAs* were biased toward symmetric divisions. Phenotypic severity correlated with hairpin strength, eliciting greatest effects with *shLGN-1617* and *shNuma1-1070*.

Since ACD spindle rotations typically occur at metaphase,9,24–26 we analysed division planes in late mitosis after commitment to a division axis. To confirm that the apical daughter remains suprabasal and differentiates following an ACD, we further monitored ACD progeny with a short BrdU pulse protocol, detecting BrdU^{+};K5^{hi}/K5^{low} doublets in *shScramble* but not *LGN*-depleted epidermis. The predominantly parallel divisions observed in ACD knockdowns did not seem to result from a developmental delay. Moreover, the effects of these knockdowns were cell-autonomous, since within mosaic tissue, RFP^{neg} cells displayed the normal ACD bias of wild-type cells. Chi-square statistical analyses confirmed that patterns of asymmetric:symmetric:oblique divisions achieved with each *LGN/Numa1/Dctn1* hairpin were significantly different ($p<0.05$) than controls (Supplementary Fig. 3).

Given that LGN, Gαi and NuMA function together in other systems,15–18 we next sought to test the interdependence of their cortical localisations in developing epidermis. In wild-type mitotic basal cells, Gαi3 and LGN showed tight co-localisation with a mean (±SD) radial difference in orientation angle of only 5.3±3.9° (n=54), and a statistically significant degree of correlation by paired t-test ($r=0.9561$, $p<0.0001$) (Fig. 1b; Supplementary Fig. 4). Both Gαi3 and LGN showed strong apical bias, with median orientation angles of 82° for Gαi3 and 80° for LGN. When either *Dctn1* or *Numa1* was depleted, LGN and Gαi remained cortically localised; however, cortical localisation of NuMA required *LGN* (Fig. 1h,i), revealing a pathway hierarchy (Gαi>LGN>NuMA). Importantly, Gαi3 remained apical in *shLGN-1617* mitotic basal cells (median orientation angle=80°, n=15), and apical positioning of interphase centrosomes, Par3 and aPKC remained unchanged (Supplementary Fig. 4). Thus, apicobasal polarity was maintained following *LGN*, *Numa1*, or *Dctn1* depletion.

Since NuMA is thought to link astral microtubules to cortical LGN,27 we tested whether upon *Numa1* knockdown, Gαi/LGN would become mislocalised. In wild-type basal keratinocytes, LGN's cortical localisation and (indirect) association with centrosomes commenced at early prophase. As one centrosome moved away in prometaphase9, LGN positioning varied, suggesting that the spindle fluctuates at this time (Supplementary Fig. 4). Cell cycle-dependent LGN localisation and metaphase flux were also observed in *Numa1* knockdowns. However, in contrast to controls, centrosomes of *Numa1* knockdown cells often appeared misaligned with the LGN cortical domain (Fig. 1j,k). These data demonstrate that proper spindle orientation depends upon coupling of LGN to NuMA.

Proper epidermal architecture requires ACDs

We next examined consequences of impairing ACDs to epidermal differentiation. In 50μM Ca^{2+}-medium, cultured keratinocytes mimic "symmetric division" mode, typified by basal keratin expression and monolayer growth. Shifting to 1.5mM Ca^{2+} favours "asymmetric divisions", characterised by epidermal sheet formation, stratification, and induction of differentiation markers. Asymmetric LGN correlated with differentiation-promoting behaviour, as LGN was polarised in >90% of mitoses in high-Ca^{2+}, compared to only ~39% in low-Ca^{2+} (n=100). Following *LGN* depletion, calcium-shifted keratinocytes still organized into sheets, but failed to form LGN crescents, stratify or differentiate. This differentiation defect was rescued by a hairpin-resistant *LGN* (Fig. 2a; Supplementary Fig. 5).

To assess whether similar differentiation defects occur *in vivo*, we examined *LGN*, *Numa1*, and *Dctn1* knockdown embryos at E17.5–E18.5, when epidermal maturation typically nears completion. Outside-in dye exclusion assays28 revealed impaired barrier function, even with the hairpin (*shDctn1-1721*) displaying the weakest spindle orientation defect (Fig. 2b). These defects were most notable in head and extremities where transduction rates were highest.19 Histological analyses revealed fewer suprabasal (differentiated) cells and ~36% more basal cells/unit area, producing a significantly thinner epidermis (Fig. 2c–e). Morphological defects were paralleled by diminished immunostaining for early (K10), intermediate (involucrin) and late (loricrin) differentiation markers (Fig. 3a,b). Mosaic embryos provided built-in controls, revealing differentiation defects specifically in RFP^+ epidermis irrespective of the ACD gene targeted (Fig. 3b).

We next traced the temporal origins of these anomalies (Supplementary Fig. 6). At E15.5, both *shLGN-1617* and wild-type epithelium displayed a single $K5/K14^+$ basal layer overlaid with sparse $K10^+$ suprabasal cells. Nonetheless, even at this early age, a thinner epidermis was evident, and by E16.5, terminal differentiation was clearly suppressed. At birth, *shLGN1617* pups displayed rough, shiny skin. As expected, the weaker hairpin *shLGN-781* caused milder abnormalities, and *shScramble* controls developed normally. Newborn *shLGN1617* pups began losing weight and died soon afterwards. Such features reflected compromised barrier function, which results in dehydration.

These defects were directly attributable to *LGN*-deficiency, and were largely rescued by resupplying a hairpin-resistant mRFP1-tagged full-length LGN on an *LGN*-knockdown background (Fig. 3c,d). However, the compromised skin phenotype of *shLGN-1617* pups

was at seeming odds with the viability of mice homozygous for an *LGN* mutation lacking the last three coding exons.21 To address whether the resulting LGNΔC might possess partial function, hence accounting for the difference, we engineered our *shLGN-1617* hairpin lentivirus to co-express a hairpin-resistant form of *mRFP1-LGNΔC*. When transduced into embryos, mRFP1-LGNΔC, but not mRFP1 alone, improved *shLGN-1617*-mediated defects in skin thickness and terminal differentiation. Although LGNΔC was not as effective as LGN-FL in rescuing *shLGN-1617*-mediated defects, both appeared to be asymmetrically segregated during ACD (Supplementary Fig. 6). Taken together with the gross normality of newborn *shLGN-781* pups, these findings suggest that partial *LGN* loss-of-function can be tolerated, while severe loss-of-function results in dehydration and death.

While LGNΔC lacks a Gαi-interacting domain, its cortical association might still be mediated through mInsc.4 Indeed, lentiviral EYFP-mInsc formed apically-oriented cortical crescents with LGN and Gαi3 in mitotic basal cells, and LGN colocalised with EYFP-mInsc with a mean (±SD) radial difference in orientation angle of 2.7 ± 2.3° ($r=0.9828$, $p<0.0001$ by paired t-test) (Fig. 3e; Supplementary Figs. 6, 7). Importantly, while LGN was normally detected in only ~75% of mitotic cells (n=80), EYFP-mInsc resulted in LGN colocalisation in 100% of mitoses (n=36).

If mInsc helps recruit LGN and mediate its effects, then elevating mInsc in wild-type embryos should enhance ACDs.29 To test this, embryos were infected with *shScramble;EYFP-mInsc*, and the division axis was quantified for $EYFP^{+}$ and $EYFP^{neg}$ mitotic cells. Like transgenic mInsc9, lentiviral EYFP-mInsc increased ACDs ($p=0.0196$ by Chi-square). Importantly, this shift required *LGN*, since predominantly symmetric divisions occurred in embryos infected with an *shLGN-1617;EYFP-mInsc* lentivirus (Fig. 3f; Supplementary Fig. 7c).

EYFP-mInsc remained apical upon *LGN* depletion. However, Gαi3 and EYFP-mInsc were often reduced in *shLGN-1617* mitotic cells, suggesting that this complex is more stable when all three components are present (Fig. 3e; Supplementary Fig. 7). Interestingly, these spindle orientation alterations also caused differentiation perturbations, as *shLGN-1617;EYFP-mInsc* epidermis was thinner than littermate cohorts, while *shScramble;EYFP-mInsc* epidermis was thicker (Figs. 3g,h). Thus suprabasal differentiation can be either promoted or impaired in an LGN-dependent manner, by a shift toward asymmetric or symmetric divisions, respectively.

In neural progenitors, the LGN homolog AGS3/Gpsm1 regulates ACDs in a Gαi-dependent fashion.30 While expressed in developing epidermis, AGS3 did not polarise at mitosis, and upon *AGS3* knockdown, LGN still localized properly, asymmetric and symmetric divisions were balanced, and differentiation seemed normal. Moreover, co-depletion of *AGS3* did not enhance the *LGN*-knockdown phenotype, and unlike *LGN*, *AGS3* knockdown *in vitro* did not perturb calcium-induced differentiation (Supplementary Fig. 8). These results show that LGN is non-redundant in skin and further underscore the specificity of the LGN/NuMA/Dctn1 pathway in causing the defects we describe.

ACDs promote Notch signalling

LGN/Numa1 knockdown did not result in abnormalities in proliferation or apoptosis (Supplementary Fig. 9). In searching elsewhere for potential causes of differentiation defects, we investigated whether Notch signalling might be altered. In mammalian epidermis, Notch is an important effector of differentiation,31–36 and in *Drosophila* neuroblasts, it is activated in the differentiating daughter.37–39 Therefore, we tested whether 1) components of the Notch pathway show abnormal expression patterns in ACD knockdowns, 2) Notch activity is altered upon *LGN*/*Numa1* depletion, and 3) Notch acts genetically in a common pathway with, and downstream of, the ACD machinery.

Microarray and RT-qPCR revealed the changes in Notch signalling that normally occur at the basal/suprabasal juncture (Fig. 4a). In agreement with and extending prior observations, 31,32,40 Notch ligands Dll1 and Jag2 were enriched basally, while suprabasal cells expressed Notch2 and Notch3 receptors, along with Jag1 ligand and Hes1, a well-known Notch target. The Notch inhibitor Numb plays a role in ACDs in *Drosophila* neuroblasts, and in adult tail skin basal keratinocytes, Numb has been reported to be asymmetrically localized.38,41–45 However, while Numb overexpression generated a mild differentiation defect in embryonic epidermis, Numb was not consistently partitioned differentially in ACDs (Supplementary Fig. 10). That said, suprabasal Hes1 was significantly reduced in *ACD* knockdowns and restored by *mRFP1-LGN* rescue. Additionally, Notch3 (and to a lesser extent Notch1 and Notch2), were reduced following *LGN* knockdown (Fig. 4b–d; Supplementary Fig. 11). These data imply that suprabasal Notch activity is diminished upon loss of *LGN*.

To measure this, we introduced a Notch reporter46 into the lentiviral shRNA backbone (Fig. 4e). The reporter was designed so that transduced cells are RFP^+, and EGFP intensity reflects reporter activity. When tested *in vitro*, the reporter harbouring *shScramble* showed the anticipated minimal Notch activation under basal conditions, but strong elevation of EGFP following a switch to differentiation-promoting, high-Ca^{2+} medium. By contrast, *shLGN1617*-transduced keratinocytes failed to induce robust reporter activity (Supplementary Fig. 11).

To test the physiological relevance of these findings, we first validated Notch reporter specificity in mouse embryos that were conditionally-defective for *RBPJ*, the obligate DNA binding partner of Notch intracellular domains (NICDs). As expected, within suprabasal layers where Hes1 and NICDs are active, transduced embryos (RFP+) showed EGFP induction only in control and not *RBPJ*-null epidermis (Fig. 4f). Similarly, the $RFP^+/EGFP^+$ co-labelled patches seen in *shScramble;Notch reporter*-transduced epidermis were markedly diminished upon *LGN* or *Numa1* knockdown (Figs. 4g,h). Analogous results were observed when Notch reporter transgenic mice46 were transduced with *shLGN-1617;H2B-mRFP1* lentivirus (Fig. 4i). As with Hes1, this decrease in reporter activity was partially restored by resupplying either *mRFP1-LGN* or *mRFP1-LGNΔC* (Supplementary Fig. 11).

Genetic interaction between ACD and Notch pathways

The poorly differentiated epidermis generated by *LGN*/*Numa1*/*Dctn1* knockdown resembled *RBPJ* conditional ablation.32 If RBPJ/Notch signalling lies downstream of ACD machinery in a common genetic pathway, then 1) ACDs should still occur in *RBPJ* mutants, 2) reducing *LGN* should not enhance *RBPJ*-mutant phenotypes, and 3) restoring active Notch signalling should partially rescue *LGN* knockdown phenotypes.

We addressed the first issue by quantifying division axis and LGN crescent orientation in mitotic cells in $RPBJ^{fl/fl}$ and $RBPJ^{fl/fl}$;*K14-Cre* embryos. To compromise Notch signalling even earlier in skin development, E9.5 $RPBJ^{fl/fl}$ embryos were transduced with *NLS-Cre-mRFP1* lentivirus. In each case, asymmetric LGN segregation was maintained, and asymmetric:symmetric divisions were balanced. This placed ACD upstream of, or parallel to, the Notch pathway (Fig. 5a–c; Supplementary Fig. 12).

To determine whether LGN and Notch act in common or independent pathways, we compared the phenotype of each single mutant to *shLGN-1617*;*RBPJ* double mutants. To this end, $RBPJ^{fl/fl}$ embryos were co-infected with *NLS-Cre-mRFP1* and either *shScramble* or *shLGN-1617* lentiviruses. *shLGN-1617*;*NLS-Cre-mRFP1;*$RBPJ^{fl/fl}$ embryos showed similarly impaired differentiation to single *shLGN-1617* and *shScramble;NLS-Cre-mRFP1;*$RBPJ^{fl/fl}$ mutants, confirming that ACD is epistatic to Notch (Fig. 5d,e).

Finally, to address whether Notch signalling is the major downstream effector of the ACD machinery, we tested whether the *shLGN-1617* loss-of-function phenotype could be rescued by restoring Notch signalling suprabasally. We utilized heterozygous *Lox-stop-Lox-Rosa-NICD-IRES-GFP* knock-in mice,47 which express active Notch (NICD) following Cre-mediated recombination. By infecting embryos with *shLGN-1617;H2B-mRFP1* ± *NLS-Cre*, we generated clones of cells expressing *shLGN-1617*, NICD, or both. Consistent with our earlier observations, proper expression of differentiation markers K10/loricrin required LGN. However, NICD overexpression at this age (E16.5) revealed appreciable cell-autonomous rescue of *shLGN-1617* differentiation defects when suprabasal Notch signalling was restored (Fig. 5f–h). These data provide compelling evidence that ACD and Notch signalling act in a common pathway promoting the basal to suprabasal switch in differentiation.

Discussion

In this study, we utilized a novel *in vivo* RNAi-based knockdown approach to systematically dissect a genetic pathway necessary to execute ACDs in developing epidermis—information which would have taken years of intensive labour to achieve by conventional mouse targeting. Moreover, our studies unveiled for the first time critical functions for *Numa1*, *Dctn1* and *LGN* in mammalian development. Specifically, they demonstrated that these ACD components act by reorienting mitotic spindles to achieve perpendicular divisions, which in turn promote stratification and differentiation. Moreover, the resemblance between these knockdown phenotypes and *RBPJ* loss-of-function mutants provided important clues that suprabasal Notch signalling is impaired when ACDs do not occur. Our findings suggest that ACDs function not only to promote stratification but also to stimulate differentiation by

enhancing compartmentalisation of Notch signalling suprabasally. In the future, this methodology should unearth additional details underlying how ACD regulates Notch signalling and orchestrates terminal differentiation. Overall, our data provide critical insights into how positional cues arising at the cell cortex regulate mitotic spindle orientation, and how coordinated actions of components of this pathway maintain the balance between stem cell proliferation and differentiation.

Methods Summary

A detailed description of the ultrasound-guided lentiviral injection procedure and production of high-titre lentiviruses is described elsewhere.19 For the present study, we used the following controls as comparisons to knockdown tissue: 1) age-matched embryos infected with a non-targeting "scramble" shRNAs (*shScramble*) which activates the endogenous miRNA processing pathway, but is not predicted to target any known mouse gene, 2) uninjected littermates, and 3) RFP^{-} (non-transduced) regions of mosaic injected embryos. All controls gave similar results, and thus they are used interchangeably in the text, though the nature of the specific control is always indicated.

RT-qPCR was performed using Absolutely RNA isolation kits (Stratagene), and Superscript VILO or III reverse transcriptase (Invitrogen) on a Roche LightCycler 480 using *Ppib* and *Hprt1* as reference genes. Immunohistochemistry was performed on fresh-frozen cryosections (8–10 μm) except in the case of the Notch reporter, where tissue was prefixed before embedding in OCT in order to preserve the GFP signal. Imaging was performed on a Zeiss Axioplan 2 epifluorescent or Zeiss LSM510 confocal microscope, with images acquired and analyzed using MetaMorph. FACS isolation was performed on a BD Aria2 equipped with 355, 405, 488, 561 and 640nm lasers, and analyses were performed on a BD LSRII. Sequences of all shRNAs used, qPCR oligonucleotides, antibodies, and mouse strains are provided in Supplementary Methods.

Figures were prepared using Adobe Photoshop and Illustrator CS5. Graphing and statistical analyses were performed using Prism 5 (GraphPad Software) and Origin 8.1 (OriginLabs).

Methods

Mice

CD1 mice from Charles River labs were used for all experiments. Notch Reporter transgenics46 were obtained from Jackson laboratories (strain Tg(Cp-EGFP)25Gaia/J, stock #005854) and outbred over multiple generations to the CD1 background, where they were maintained as homozygotes. Homozygous *Lox-stop-Lox-Rosa*$^{NICD\text{-}IRES\text{-}GFP}$ male breeder mice47 were obtained from Jackson laboratories (strain Gt(ROSA)26Sortm1(Notch1)Dam/J, stock #008159) and crossed to CD1 females when used for lentiviral injections. *RBPJ*$^{fl/fl}$ mice48 were bred as homozygotes for lentiviral injections, or crossed to *K14-Cre*49;*RBPJ*$^{fl/+}$ females for analyses of the conditional mutant phenotype. BrdU (50 μg/g) was injected intraperitoneally to pregnant females 4–6h before sacrificing by administration of CO_2. All animals were maintained in an AAALAC-approved animal facility and procedures were performed using IACUC-approved protocols.

Constructs and RNAi

All shRNAs except *shDctn1-1721* were obtained from The Broad Institute's Mission TRC-1 mouse library, and were present in the pLKO.1 lentiviral backbone, which harbours a puromycin-resistance cassette. shRNA sequences were cloned from the library vectors into our modified pLKO H2B-mRFP1, H2B-YFP, or H2B-CFP vectors.19 The lentiviral Notch reporter was generated by cloning a KpnI-XbaI fragment containing the 4 CBF1 binding elements, SV40 minimal promoter, and EGFP from Addgene clone 1770546 into pLKO *shScramble*;*H2B-mRFP1* or *shLGN-1617*;*H2B-mRFP1*. For expression of EYFP-mInsc, mRFP1-Numb, and mRFP1-LGN (FL and ΔC), the pLKO backbone was modified to delete the puromycin-resistance gene following the PGK promoter, and replace it with a custom multiple cloning site (pLKO PGK MCS). This facilitated subsequent cloning and allowed the use of a single lentivirus that could both express a cDNA of interest and an shRNA. The 72kD Numb isoform was cloned from mouse cDNA by PCR and fused to mRFP1, while EYFP-mInsc was reported previously.7 LGNΔC was produced according to the published mutant,21 which lacks exons 13, 14, and the coding region of the last exon 15. This truncates the protein at aa474, deleting the GoLoco motifs that mediate LGN's interaction with Gαi/Gαo. It was also empirically found to delete the epitope for our LGN antibody (see below), which was raised to the C-terminus.

Viruses were produced as described19. The following shRNAs were used: *shLGN-1617* (TRCN0000028914), *shLGN-781* (TRCN0000028914), *shNuma1-1070* (TRCN0000037190), *shNuma1-6790* (TRCN0000072130), *shDctn1-289* (TRCN0000072128), *shAGS3-759* (TRCN0000037192), *shAGS3-1147* (TRCN0000037192), *shScramble* (Sigma SHC002). Detailed maps and constructs are available upon request. Full hairpin sequences (minus AgeI and EcoRI cloning sites) are listed below:

shScramble	CAACAAGATGAAGAGCACCAACTCGAGTTGGTGCTCTTCATCTTGTTG
shLGN-1617	GCCGAATTGGAACAGTGAAATCTCGAGATTTCACTGTTCCAATTCGGC
shLGN-781	GCGCTCTACAATCTTGGAAATCTCGAGATTTCCAAGATTGTAGAGCGC
shNuma1-1070	GCCAGATGGATCGAAAGATTACTCGAGTAATCTTTCGATCCATCTGGC
shNuma1-6790	CCTTAGTCTCTGGACCTAGAACTCGAGTTCTAGGTCCAGAGACTAAGG
shDctn1-289	CCAGTCCCAGATCCAAGTATTCTCGAGAATACTTGGATCTGGGACTGG
shDctn1-1721	GCCATTGAGATGGAGTTGAGACTCGAGTCTCAACTCCATCTCAATGGC
shAGS3-759	CCACTACCTACTGGGAAACTTCTCGAGAAGTTTCCCAGTAGGTAGTGG
shAGS3-1147	GCCTTGACCTTTGCCAAGAAACTCGAGTTTCTTGGCAAAGGTCAAGGC

Cell Culture

Primary mouse keratinocytes were maintained in E medium with 15% FBS and 50 μM $CaCl_2$ (low Ca^{2+} medium). For viral infections, keratinocytes were plated in 6-well dishes at 100,000 cells per well and incubated with lentivirus in the presence of polybrene (100 μg/mL). After 2d, we positively selected infected cells with puromycin (1–2 μg/mL) for 4–7 d, and processed them for mRNA and protein analyses. Calcium shift assays were performed

as follows. Keratinocytes were seeded at a saturating density (200,000 cells/24-well) onto coverslips coated with collagen and fibronectin. Cells were switched to high Ca^{2+} (1.5 mM) medium 16–24 h later, and grown for the indicated period of time (24–72 h). Cells were fixed with 4% paraformaldehyde for 10 min at RT. Immunostaining was performed using the same protocol as for slides (below). As differentiation is sensitive to cell density, nuclei/field were quantifed using Metamorph and only images with between 1800–2000 nuclei/10× field were quantified for K10 expression.

Antibodies, Immunohistochemistry and Imaging

Antisera against LGN were raised in guinea pigs using the C-terminus (aa 376–572) of LGN fused to GST, and were affinity purified using HiTrap NHS columns conjugated to purified immunogen protein (Pierce). Embryos were either embedded whole (<E16.5) or skinned and flat-mounted on paper towels. Both infected and littermate controls were embedded together in a single block to control for potential variability in immunostaining conditions. Embryos and skin were embedded unfixed in OCT (Tissue Tek), except for Notch reporter sections, which were prefixed for 1h in 4% paraformaldehyde in order to preserve the cytoplasmic GFP signal. To detect the reporter, antibodies against GFP were used, coupled to either fluorescent secondary antibodies or POD-conjugated secondaries which were amplified using the TSA Plus fluorescein or Cy5 system (Perkin Elmer). For BrdU immunostaining, slides were treated with 1N HCl for 1 h at 37°C before adding the anti-BrdU antibody.

Frozen sections were cut at a thickness of 8–10 μm on a Leica cryostat and mounted on SuperFrost Plus slides (Fisher). Slides were air-dried for 30 minutes, then fixed for 10 minutes with 4% paraformaldehyde, rinsed with PBS, then blocked for 1 h in gelatin block (5% NDS, 1% BSA, 2% gelatin, 0.2% triton-X in PBS) or BSA/NDS block (3% BSA, 5% NDS, 0.2% triton-X in PBS) before incubating in primary antibody diluted in block at 4°C overnight. After washing with PBS, secondary antibodies, conjugated to Alexa-488 (Molecular Probes), Cy3, RRX, DyLight 549, or Cy5 (Jackson Laboratories), were added for 1–2 h at RT. Slides were washed, counterstained with DAPI (0.5 μg/mL) and mounted in ProLong Gold (Invitrogen). Imaging was performed on a Zeiss Axioplan 2 using 10×/0.45 air, 20×/0.8 air, 63×/1.4 oil, or 100×/1.4 oil Plan-Apochromat objectives and the following Chroma filter sets: 49003 ET YFP (YFP), 49008 ET TR C94094 (mRFP1), 49004 ET dsR C94093 (Cy3, DyLight 549), 41008 Cy5 (Cy5), 41001 FITC (AlexaFluor 488/GFP); or a Zeiss LSM 510 Meta scanning confocal microscope with 40×/1.2 air or 63×/1.4 oil objective.

The following primary antibodies were used: Mouse IgM anti-NuMA (BD Biosciences, 1:200), Rb anti-pericentrin (Covance, 1:500), Rb anti-Gαi3 977 (gift of T. Gettys, 1:400), Rb anti-RFP (MBL, 1:4000), Rb mAb anti-survivin (Cell Signaling, 1:400), GP anti-K5 (Fuchs lab, 1:200), Rt mAb anti-Ecad (Fuchs lab, 1:500), Rb anti-K10 (Covance, 1:1000), Rb anti-K14 (Fuchs lab, 1:500), Rt anti-CD104/β4 integrin (BD Pharmingen), Rb anti-loricrin (Fuchs lab, 1:1000), Rb anti-involucrin (Covance, 1:1000), Rb anti-filaggrin (Covance, 1:1000), Rb anti-Hes1 (Fuchs lab, 1:500), Chicken anti-GFP (Abcam, 1:5000), Rb anti-GFP (Invitrogen, 1:5000), Hamster mAb anti-Notch3 (Biolegend, 1:400), Rb anti-Notch3/NICD3 (Abcam ab23426, 1:400), Mouse mAb anti-acetylated tubulin (Sigma,

6-11B-1, 1:400), Rb anti-γtubulin (Abcam, 1:500), Mouse mAB anti-βtubulin (Sigma, TUB 2.1, 1:500), Rb anti-AGS3 pep32 (gift of S. Lanier, 1:500), Rb anti-AGS3 pep22 (S. Lanier, 1:200), Rb anti-aPKC (Santa Cruz, N-17, 1:200), Rb anti-Par3 (Upstate/Millipore, 1:500), Rt anti-HA (Roche, 1:200), Rt anti-BrdU (Abcam, 1:200), Rb anti-RFP-HRPDirecT (MBL, 1:2000), Goat anti-Dctn1 (Abcam ab11806, 1:500).

RT-qPCR

mRNA was isolated using Absolutely RNA miniprep or microprep kits (Stratagene), and was quantified using a Nanodrop spectrophotometer. cDNA was synthesized from 2–500 ng of total RNA using either Superscript III with oligo-dT primers or Superscript VILO with random-primers (Invitrogen). Real-time qPCR was performed on a LightCycler 480 (Roche), and relative quantification performed using Roche software, with data normalized relative to *cyclophilin* (*Ppib*) and *Hprt1* (using the geometric mean of the Cp values from both reference genes). To confirm the functionality of the primer sets used, multiple primer pairs were designed and tested for each gene; efficiencies of primer pairs were determined empirically (>1.8); specificity confirmed by the absence of product in samples prepared without reverse transcriptase (−RT controls), and product sizes calculated by melting curve analysis and confirmed by gel electrophoresis. The following primer sequences were used:

	Forward primers	**Reverse primers**
LGN	TCTGCTGCAAAGAGATCCAAACA	TCATGGGCAGGTACAAAAAGTCC
	TCCCCCAACACAGATGAGTTCTT	ATCTTGACCCCTGGCACTTTACA
Numa1	GTCAGGCCCCCTTGGAGACT	AGCGGGCCAGAGACTGAGTG
	CGGGAGCTGGAGGTGATGAC	TCAGACCGCAGCTCCTTGTTC
Dctn1	GTGCGGGAGTTACGGGAGACT	GCCTGGGCAACTTCCATCTG
	CCTCCAGCAGCCCCTATGAGT	CTCGTCCAGCCGTGTCTGAAC
AGS3	TTGGGGAGGCGAGAGCACT	AGCGCCCCAAGAAGATGTGA
	GAGCCGGGGGATGAGTTTTT	ATCATGGCCTTGGGAAGATTTG
K14	CGCCGCCCCTGGTGTGG	ATCTGGCGGTTGGTGGAGGTCA
K10	GGAGGGTAAAATCAAGGAGTGGTA	GGAGGGTAAAATCAAGGAGTGGTA
Loricrin	GTAAGGTCACCGGGTTGCAA	GCTTAAAATGTGAAGGGTTTGGAA
Notch1	CAAACTGGCCTGGGTGGGGACAT	AAAAGGCCAGAAAGAGCTGCCCTGAG
Notch2	GCAGCCGGAGCTCCCCAGACG	GTCCCCGCTGACCGCCTCCAC
Notch3	TGAGCTTGGGAAATCTGCCTTACA	CTTCTTGCCCCGACCACGAGTTCC
	ACATGGCCAAGGGTGAGAGTCT	GCTGGGCCCCTTGACAGAT
Notch4	TGACACGGGCTCCTCCTATTTC	CAGTAGAAGGCGTTGGCTAAAGAGT
	CGACGCTCGGGAGGTTTG	AAGCGGCGTCTGTTCCCTACT
Dll1	TGCGGCTCTTCCCCTTGTT	TGGCAGGTGGCCCCATTA
	GAAGCCACGGTCAGGGATACA	GTCGGGCGCCTCTGCTAA
Dlk1	CAGCGGCAACGGAAGTCAC	ACTGCCCCTGGCTGTGTCA
Dll3	ATGGGCGTGAGATGCGAGTT	GGGGCTGGTATGACATAAATGGAT
Jag1	ACCCTGTCAAGGAAATTACCGATAA	CTTCCGCCGCTTCCTTACAC
	GTGGCTGGGAAGGAACAACCT	TGGCCCCAAAGGCACAAG

	Forward primers	Reverse primers
Jag2	GAGGGCGGCGGCACACGAC	CCGGCCTGGCCGCTCAATGG
Hes1	AGAAGAGGCGAAGGGCAAGAA	CATGGCGTTGATCTGGGTCAT
	AGTGGTGCCGGCTCCTGA	TTCCGCCACGGTCTCCAC
Numb	AGTGCCCGAGGTGGAAGGA	GCCCGCACACTCTTTGACACT
	CTCGGCCACGTAGAAGTTGATG	CACTCCTTCTCCCGCTTCTGTT
Numbl	CACCAGTGGCAGGCAGATGA	GTCGCGGCATATGTAGGAGAAAG
	CGCACGGACTTCCAGGTGA	CGGCAGGAAAACAGCCACTT
Ki67	CCCAGCTCGTCTCCACCACTAGAG	TCTGTGTGTTTCTGGTTTGCCTTAC
	GGCGTGAAACAAACACAAACGAAAG	CTGTGGTGATGGGCTCAGGTATGTC
Ccna2	TGTAGGCACGGCTGCTATGC	GTTGTGGCGCTTTGAGGTAGG
Ccne2	CTGCTGCCGCCTTATGTCATT	CAGCTGCCCTCCTTTTCTGTAGA
	AAACTGTGCTCTAAATGGGAGAACC	ATATGGGGCTTAAAAATGGACCAC
Ccnb1	CCCCCAAGTCTCACTATCAACAGA	GTGGCGCCTTGGTATGGTG
Ccnd1	TGTGCGCCCTCCGTATCTTAC	TTCTCGGCAGTCAAGGGAATG
	TCGCTGCTATTGGAGGGTCAG	CACAACAGGCCGCTACAAGAAA
Bax	GACAGGGGCCTTTTTGCTACAG	CTGATCAGCTCGGGCACTTTAGT
Bbc3	GAGCGGCGGAGACAAGAAGA	CACCAGCAGCCTTTCCTGAGA
	CACCAGCCCAGCAGCACTTA	TCGTACTGCGCGTTGAGGTC
Noxa	CGCAGATGCCTGGGAAGTC	CCAAAAGCAAGCGAGCGTTTCTCT
Hprt1	GATCAGTCAACGGGGGACATAAA	CTTGCGCTCATCTTAGGCTTTGT
Ppib	GTGAGCGCTTCCCAGATGAGA	TGCCGGAGTCGACAATGATG

Western Blotting

Gel electrophoresis was performed using 4–12% NuPAGE Bis-Tris gradient gels (Invitrogen), transferred overnight at 100 mA to nitrocellulose membranes. Membranes were blocked for 1h in Odyssey blocking buffer (LI-COR), then incubated with primary antibodies in Odyssey block + 0.1% Tween-20 overnight at 4°C with gentle agitation. Membranes were rinsed several times in PBT (PBS + 0.1% Tween-20) before incubating in secondary antibodies diluted in Odyssey block for 30 minutes at RT in the dark. Membranes were washed in PBT, then in PBS before imaging on a LiCor infrared scanner. Quantification of band intensities was performed using Odyssey 3.0 software. Primary antibodies used were: GP anti-LGN (Fuchs lab, 1:2000), Rb anti-LGN (S. Bahria, 1:2000), Mouse IgG anti-βactin (Sigma, 1:5000), Rb anti-Hprt1 (Abcam, 1:2000). Secondary antibodies were conjugated to IRDye680 or IRDye800CW (LiCor and Rockland), and were used at 1:15000.

Flow Cytometry

Embryos from K14H2B-GFP$^{+/+}$ male × CD1 female matings, injected with lentivirus at E9.5, were collected at either E15.5 or E18.5 and processed as follows. For E15.5 embryos, back and head skin were dissected, and digested in 0.25% collagenase (Sigma) in HBSS for 1 h at 37°C with intermittent trituration and shaking. Epidermis was separated from dermal fibroblasts by filtering through a 70 μm filter and collecting the retaining epidermis. For

E18.5 embryos, back and head skin were dissected and treated with dispase for 1 h at 37°C with shaking. The epidermis was peeled away from the underlying dermis using fine forceps. Isolated collagenase- or dispase-treated epidermis was then treated with 0.25% Trypsin-EDTA (Invitrogen) for 15 mins at RT with shaking. Keratinocytes were isolated by filtering through a 70μm cell strainer, retaining the flow-through cell suspension. PBS + 1% FBS (treated with BioRad Chelex to remove calcium) was added to inactivate trypsin, and cells were collected by centrifugation for 5 minutes at 300 × g. Cell pellets were resuspended in PBS + 1% FBS and stained with CD49f/α6 integrin-Alexa647 (AbD Serotec) diluted 1:50 for 30 minutes on ice. DAPI (20 ng/mL) was used for live/dead exclusion. FACS isolations were performed on a BD FacsAria 2 equipped with 355, 405, 488, 561, and 640nm lasers. Cells were gated as $a6^{hi}$ (basal) and $a6^{low}$ (suprabasal), and sorted for $GFP^{+}RFP^{+}$ (transduced, knockdown) and $GFP^{+}RFP^{-}$ (internal control) populations. $GFP^{+}RFP^{-}$ littermates were also sorted as controls. Sorted cells were validated by post-sort analysis on a BD LSR II; and RFP, GFP and α6 integrin expression assessed by RT-qPCR on RNA isolated from sorted populations. Sorted cells were divided for protein, RNA, and cell cycle analyses.

For cell cycle analyses, ~200,000 cells were resuspended in 150 μL of PBS, then fixed by drop-wise addition of 4 volumes of ice-cold 100% EtOH while vortexing. Cells were fixed for 15 minutes on ice, and stored at 4°C. After fixation, cells were centrifuged for 5 mins at 1000 × g, resuspended in PBS, and centrifuged again. Cells were resuspended in propidium iodide solution (10 μg/mL) with RNAse A (250 μg/mL), and stained for 15 minutes at 37°C in the dark. Cell cycle analysis was performed on a BD LSR II, and data processed and graphed using FlowJo 8.8.4.

Histology and electron microscopy analysis

Skin samples were fixed in 2% glutaraldehyde, 4% PFA, and 2 mM $CaCl_2$ in 0.05 M sodium cacodylate buffer, pH 7.2, at RT for >1 h, postfixed in 1% osmium tetroxide and processed for Epon embedding; semi-thin sections (1 μm) were stained with toluidine blue and examined by light microscopy. For transmission electron microscopy, ultrathin sections (60–70 nm) were counterstained with uranyl acetate and lead citrate. EM images were taken with a transmission electron microscope (Tecnai G2–12; FEI) equipped with a digital camera (Model XR60; Advanced Microscopy Techniques, Corp.).

Barrier Assay

Dye exclusion assays were performed essentially as described.28 Essentially, unfixed embryos are immersed in a low pH X-gal substrate solution (100 μM $NaPO_4$, 1.3 mM $MgCl_2$, 3 mM $K_3Fe(CN)_6$, 3 mM $K_4Fe(CN)_6$, 1mg/mL X-gal, 0.01% sodium deoxycholate, 0.2% NP-40, pH 4.5) at 30–37°C for several hours to overnight until colour develops. Tails were snipped to serve as a positive control for staining. The principle of the assay is that at low pH, skin contains abundant β-galactosidase activity, so when the epidermis has incomplete barrier function, X-gal is cleaved and the blue precipitate is deposited.

Measurements, Quantification, Graphing, and Statistics

Spindle orientation was determined by measuring the angle between the centrosomal axis and the basement membrane in late prophase and metaphase cells, when two centrosomes were observed at opposite sides of the cell (in early prophase, the centrosomal pair is localized apically). LGN orientation was determined by measuring the angle defined by a line transecting the middle of the LGN crescent through the cell center, relative to the basement membrane. Stages of mitosis were defined as follows: early prophase cells had condensed chromatin lacking a clearly-defined pair of centrosomes; late prophase cells had a pair of centrosomes positioned at opposing poles; metaphase cells resembled late prophase cells but displayed aligned chromosomes characteristic of the metaphase plate. All cells were positive for phospho-histone H3 and LGN.

Axis of division was determined in anaphase/telophase cells, as it became obvious from analyses of metaphase spindle orientation that cells at this stage were dynamic, and spindle orientation was not necessarily predictive of the ultimate plane of division. Because phospho-histone H3 staining is weak or undetectable at this stage of the cell cycle, we utilized a novel marker to identify anaphase/telophase cells. Survivin/Birc5 is a component of the chromosomal passenger complex (CPC), together with INCENP/Aurora B kinase and Borealin/Dasra B. At prometaphase/metaphase, the CPC localizes to the inner centromeres, but at anaphase it translocates to the central spindle, and then finally to the midbody during cytokinesis. We therefore found this antibody to be an effective marker for anaphase/telophase cells, as survivin was present at the midzone between two daughter nuclei, allowing us to distinguish definitively between mitotic nuclei from a single cell and closely juxtaposed nuclei from neighbouring cells (this was confirmed secondarily by using the cell membrane marker E-cadherin). Angle of division was determined by measuring the angle defined by the plane transecting two daughter nuclei relative to the plane of the basement membrane.

Backskin thickness was quantified by taking >40 measurements/embryo of RFP^+ regions from 5 random 20× fields arrayed from anterior to posterior. Epidermal thickness was measured as the distance from the basement membrane (labelled with β4 integrin) to the skin surface. Measurements of individual embryos are displayed as box and whisker plots (Fig. 2f), with the dimensions of the box encompassing the 25–75% percentile, the horizontal bar representing the mean, and the error bars representing the minimum and maximum values. These values were normalized to the mean thickness of uninfected embryos from the same litter in order to control for subtle differences in gestational age between litters. Spinous/granular layer thickness in analyses of *RBPJ* mutants and NICD rescue experiments was calculated using Metamorph. A common threshold intensity was set for K10 fluorescent intensity, creating a binary image, whose area was calculated, and divided by the length of the section to determine average thickness. 10–40 sections of head and anterior backskin were quantified for each genotype, from >3 embryos. Data presented are the mean ± SEM.

Data were analyzed and statistics performed (unpaired two-tailed student's t-tests or Chi-square tests) in Prism 5 (GraphPad). For determination of axis of cell division, the number of cells analyzed (n) is indicated in the radial histograms, and included cells from 3 or more

embryos of the same age. Radial histograms of angle of division were plotted in Origin 8.1 (OriginLab) from raw data binned into 10° increments. All other graphs were prepared in Prism.

Supplementary Material

Refer to Web version on PubMed Central for supplementary material.

Acknowledgments

We thank N. Stokes, L. Polak and D. Oristian for their expert assistance in the mouse facility; S. Lanier and T. Gettys for providing AGS3 and Gαi antibodies; N. Gaiano and C. Cepko for constructs; D. Melton and T. Honjo for mice; S. Chai for Numb constructs; E. Ezhkova for sharing microarray data; and J. Knoblich for sharing unpublished results and reagents. We are grateful to M. Schober, D. Devenport, E. Ezratty, C. Luxenburg, and members of the Fuchs laboratory for helpful discussions and critical reading of the manuscript. We thank A. North and the RU Bioimaging Resource Center for assistance with image acquisition and the Comparative Biology Center (AAALAC accredited) for veterinary care of our mice. S.E.W. was supported by an American Cancer Society postdoctoral fellowship and S.B. was a Human Frontier Science Program postdoctoral fellow. E.F. is an investigator in the Howard Hughes Medical Institute. Work in the Fuchs laboratory was supported by a grant from the National Institutes of Health (E.F. R01AR27883).

References

1. Neumuller RA, Knoblich JA. Dividing cellular asymmetry: asymmetric cell division and its implications for stem cells and cancer. Genes Dev. 2009; 23:2675–2699. [PubMed: 19952104]
2. Knoblich JA. Mechanisms of asymmetric stem cell division. Cell. 2008; 132:583–597. [PubMed: 18295577]
3. Siller KH, Doe CQ. Spindle orientation during asymmetric cell division. Nat Cell Biol. 2009; 11:365–374. [PubMed: 19337318]
4. Yu F, Morin X, Cai Y, Yang X, Chia W. Analysis of partner of inscuteable, a novel player of Drosophila asymmetric divisions, reveals two distinct steps in inscuteable apical localization. Cell. 2000; 100:399–409. [PubMed: 10693757]
5. Schober M, Schaefer M, Knoblich JA. Bazooka recruits Inscuteable to orient asymmetric cell divisions in Drosophila neuroblasts. Nature. 1999; 402:548–551. [PubMed: 10591217]
6. Wodarz A, Ramrath A, Kuchinke U, Knust E. Bazooka provides an apical cue for Inscuteable localization in Drosophila neuroblasts. Nature. 1999; 402:544–547. [PubMed: 10591216]
7. Lechler T, Fuchs E. Asymmetric cell divisions promote stratification and differentiation of mammalian skin. Nature. 2005; 437:275–280. [PubMed: 16094321]
8. Smart IH. Variation in the plane of cell cleavage during the process of stratification in the mouse epidermis. Br J Dermatol. 1970; 82:276–282. [PubMed: 5441760]
9. Poulson ND, Lechler T. Robust control of mitotic spindle orientation in the developing epidermis. J Cell Biol. 2010; 191:915–922. [PubMed: 21098114]
10. Fuchs E. Scratching the surface of skin development. Nature. 2007; 445:834–842. [PubMed: 17314969]
11. Bowman SK, Neumuller RA, Novatchkova M, Du Q, Knoblich JA. The Drosophila NuMA Homolog Mud regulates spindle orientation in asymmetric cell division. Dev Cell. 2006; 10:731–742. [PubMed: 16740476]
12. Izumi Y, Ohta N, Hisata K, Raabe T, Matsuzaki F. Drosophila Pins-binding protein Mud regulates spindle-polarity coupling and centrosome organization. Nat Cell Biol. 2006; 8:586–593. [PubMed: 16648846]
13. Siller KH, Cabernard C, Doe CQ. The NuMA-related Mud protein binds Pins and regulates spindle orientation in Drosophila neuroblasts. Nat Cell Biol. 2006; 8:594–600. [PubMed: 16648843]
14. Blumer JB, Kuriyama R, Gettys TW, Lanier SM. The G-protein regulatory (GPR) motif-containing Leu-Gly-Asn-enriched protein (LGN) and Gialpha3 influence cortical positioning of the mitotic

spindle poles at metaphase in symmetrically dividing mammalian cells. Eur J Cell Biol. 2006; 85:1233–1240. [PubMed: 17000024]

15. Woodard GE, et al. Ric-8A and Gi alpha recruit LGN, NuMA, and dynein to the cell cortex to help orient the mitotic spindle. Mol Cell Biol. 2010; 30:3519–3530. [PubMed: 20479129]
16. Du Q, Macara IG. Mammalian Pins is a conformational switch that links NuMA to heterotrimeric G proteins. Cell. 2004; 119:503–516. [PubMed: 15537540]
17. Siegrist SE, Doe CQ. Microtubule-induced Pins/Galphai cortical polarity in Drosophila neuroblasts. Cell. 2005; 123:1323–1335. [PubMed: 16377571]
18. Bernard ML, Peterson YK, Chung P, Jourdan J, Lanier SM. Selective interaction of AGS3 with G-proteins and the influence of AGS3 on the activation state of G-proteins. J Biol Chem. 2001; 276:1585–1593. [PubMed: 11042168]
19. Beronja S, Livshits G, Williams SE, Fuchs E. Rapid Functional Dissection of Genetic Networks Via Tissue-Specific Transduction and RNAi in Mouse Embryos. Nat Med. 2010; 16:821–827. Epub 2010 Jun 6. [PubMed: 20526348]
20. Morin X, Jaouen F, Durbec P. Control of planar divisions by the G-protein regulator LGN maintains progenitors in the chick neuroepithelium. Nat Neurosci. 2007; 10:1440–1448. [PubMed: 17934458]
21. Konno D, et al. Neuroepithelial progenitors undergo LGN-dependent planar divisions to maintain self-renewability during mammalian neurogenesis. Nat Cell Biol. 2008; 10:93–101. [PubMed: 18084280]
22. Zheng Z, et al. LGN regulates mitotic spindle orientation during epithelial morphogenesis. J Cell Biol. 2010; 189
23. Moffat J, et al. A lentiviral RNAi library for human and mouse genes applied to an arrayed viral high-content screen. Cell. 2006; 124:1283–1298. [PubMed: 16564017]
24. Adams RJ. Metaphase spindles rotate in the neuroepithelium of rat cerebral cortex. J Neurosci. 1996; 16:7610–7618. [PubMed: 8922417]
25. Geldmacher-Voss B, Reugels AM, Pauls S, Campos-Ortega JA. A 90-degree rotation of the mitotic spindle changes the orientation of mitoses of zebrafish neuroepithelial cells. Development. 2003; 130:3767–3780. [PubMed: 12835393]
26. Kaltschmidt JA, Davidson CM, Brown NH, Brand AH. Rotation and asymmetry of the mitotic spindle direct asymmetric cell division in the developing central nervous system. Nat Cell Biol. 2000; 2:7–12. [PubMed: 10620800]
27. Du Q, Stukenberg PT, Macara IG. A mammalian Partner of inscuteable binds NuMA and regulates mitotic spindle organization. Nat Cell Biol. 2001; 3:1069–1075. [PubMed: 11781568]
28. Hardman MJ, Sisi P, Banbury DN, Byrne C. Patterned acquisition of skin barrier function during development. Development. 1998; 125:1541–1552. [PubMed: 9502735]
29. Kraut R, Chia W, Jan LY, Jan YN, Knoblich JA. Role of inscuteable in orienting asymmetric cell divisions in Drosophila. Nature. 1996; 383:50–55. [PubMed: 8779714]
30. Sanada K, Tsai LH. G protein betagamma subunits and AGS3 control spindle orientation and asymmetric cell fate of cerebral cortical progenitors. Cell. 2005; 122:119–131. [PubMed: 16009138]
31. Watt FM, Estrach S, Ambler CA. Epidermal Notch signalling: differentiation, cancer and adhesion. Curr Opin Cell Biol. 2008; 20:171–179. [PubMed: 18342499]
32. Blanpain C, Lowry WE, Pasolli HA, Fuchs E. Canonical notch signaling functions as a commitment switch in the epidermal lineage. Genes Dev. 2006; 20:3022–3035. [PubMed: 17079689]
33. Moriyama M, et al. Multiple roles of Notch signaling in the regulation of epidermal development. Dev Cell. 2008; 14:594–604. [PubMed: 18410734]
34. Demehri S, et al. Notch-deficient skin induces a lethal systemic B-lymphoproliferative disorder by secreting TSLP, a sentinel for epidermal integrity. PLoS Biol. 2008; 6:e123. [PubMed: 18507503]
35. Pan Y, et al. gamma-secretase functions through Notch signaling to maintain skin appendages but is not required for their patterning or initial morphogenesis. Dev Cell. 2004; 7:731–743. [PubMed: 15525534]

36. Rangarajan A, et al. Notch signaling is a direct determinant of keratinocyte growth arrest and entry into differentiation. Embo J. 2001; 20:3427–3436. [PubMed: 11432830]
37. Coumailleau F, Furthauer M, Knoblich JA, Gonzalez-Gaitan M. Directional Delta and Notch trafficking in Sara endosomes during asymmetric cell division. Nature. 2009; 458:1051–1055. [PubMed: 19295516]
38. Emery G, et al. Asymmetric Rab 11 endosomes regulate delta recycling and specify cell fate in the Drosophila nervous system. Cell. 2005; 122:763–773. [PubMed: 16137758]
39. Mummery-Widmer JL, et al. Genome-wide analysis of Notch signalling in Drosophila by transgenic RNAi. Nature. 2009; 458:987–992. [PubMed: 19363474]
40. Nickoloff BJ, et al. Jagged-1 mediated activation of notch signaling induces complete maturation of human keratinocytes through NF-kappaB and PPARgamma. Cell Death Differ. 2002; 9
41. Knoblich JA, Jan LY, Jan YN. Asymmetric segregation of Numb and Prospero during cell division. Nature. 1995; 377:624–627. [PubMed: 7566172]
42. Wang H, Ouyang Y, Somers WG, Chia W, Lu B. Polo inhibits progenitor self-renewal and regulates Numb asymmetry by phosphorylating Pon. Nature. 2007; 449:96–100. [PubMed: 17805297]
43. Wirtz-Peitz F, Nishimura T, Knoblich JA. Linking cell cycle to asymmetric division: Aurora-A phosphorylates the Par complex to regulate Numb localization. Cell. 2008; 135:161–173. [PubMed: 18854163]
44. Rhyu MS, Jan LY, Jan YN. Asymmetric distribution of numb protein during division of the sensory organ precursor cell confers distinct fates to daughter cells. Cell. 1994; 76:477–491. [PubMed: 8313469]
45. Clayton E, et al. A single type of progenitor cell maintains normal epidermis. Nature. 2007; 446:185–189. [PubMed: 17330052]
46. Mizutani K, Yoon K, Dang L, Tokunaga A, Gaiano N. Differential Notch signalling distinguishes neural stem cells from intermediate progenitors. Nature. 2007; 449:351–355. [PubMed: 17721509]
47. Murtaugh LC, Stanger BZ, Kwan KM, Melton DA. Notch signaling controls multiple steps of pancreatic differentiation. Proc Natl Acad Sci U S A. 2003; 100:14920–14925. [PubMed: 14657333]
48. Tanigaki K, et al. Notch-RBP-J signaling is involved in cell fate determination of marginal zone B cells. Nat Immunol. 2002; 3:443–450. [PubMed: 11967543]
49. Vasioukhin V, Degenstein L, Wise B, Fuchs E. The magical touch: genome targeting in epidermal stem cells induced by tamoxifen application to mouse skin. Proc Natl Acad Sci U S A. 1999; 96:8551–8556. [PubMed: 10411913]

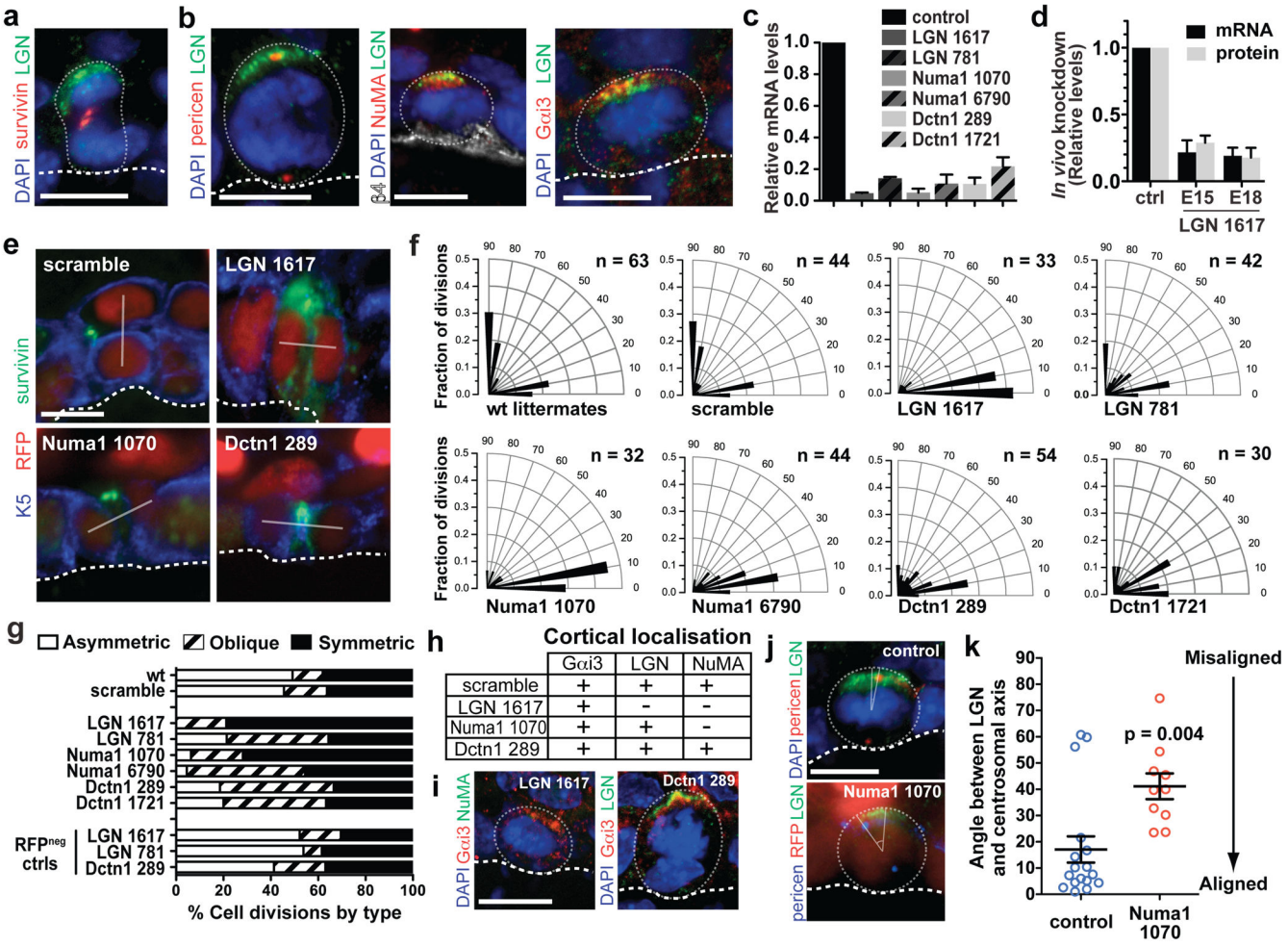

Figure 1. Spindle orientation defects following *LGN*, *Numa1*, and *Dctn1* depletion

a, Immunodetection of anaphase-telophase pronuclei. with spindle midbody marker Survivin. **b,** Apical colocalisation of ACD components during mitosis. **c,d** *shRNA* knockdown efficiencies in keratinocytes and epidermis (n=3 separate experiments). **e,** Representative axes of division (lines) in E16.5 transduced anaphase/telophase cells. **f,** Radial histogram quantification of data from **(e),** n's are indicated. **g,** Cell-autonomous elimination of ACDs upon *LGN*, *Numa1*, or *Dctn1* knockdown. **h–i,** Interdependence of Gαi3/LGN/NuMA cortical localisation. **j,k** Misalignment of angles between LGN crescent centre and centrosomal axis (spindle) upon *Numa1* knockdown (each dot indicates a single data point). Scale bars: 10μm. Error bars: S.D. (**c, d**); S.E.M (**k**). Dotted lines denote basement membrane (thick); cell boundaries (thin).

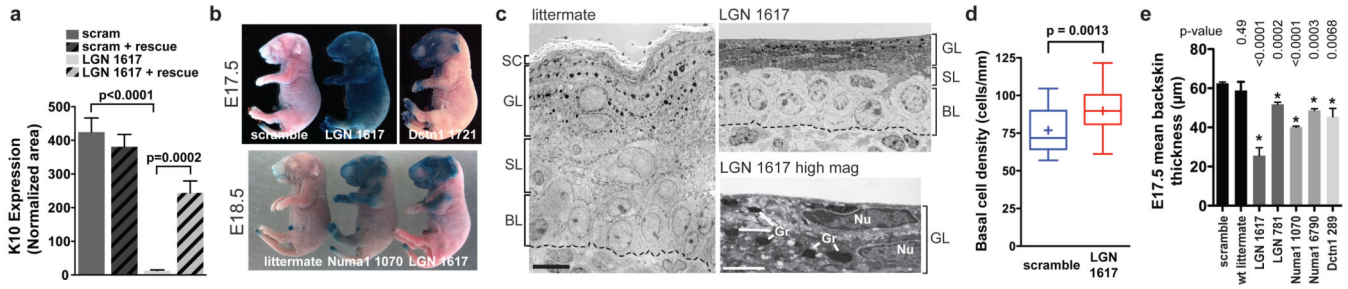

Figure 2. Impaired stratification *in vitro* and *in vivo* in when ACDs are impaired

a, Quantification of differentiation (K10) in *shLGN-1617*-transduced and rescued keratinocytes (n=8 fields/condition). **b**, Skin barrier defects in ACD knockdown embryos. **c,** Epidermal ultrastructure. Layers: BL, basal; SL, spinous; GL, granular; SC, stratum corneum (bar, 10µm).. Late-stage differentiation defects in *LGN* knockdowns are shown at higher magnification (bar, 2µm; Gr, keratohyalin-granules; Nu, nuclei). **d,** Quantifications revealing ~17% increase in basal nuclei density (~36% more basal cells/mm) in E17.5 *shLGN-1617* epidermis. Whiskers indicate minimum and maximum values; boxes span 25–75 percentiles, centre bar denotes median value; +marks designate mean, n>20 sections/condition. **e,** Measurements of epidermal thinning in knockdowns (n>3 embryos/condition). Error bars represent S.D.

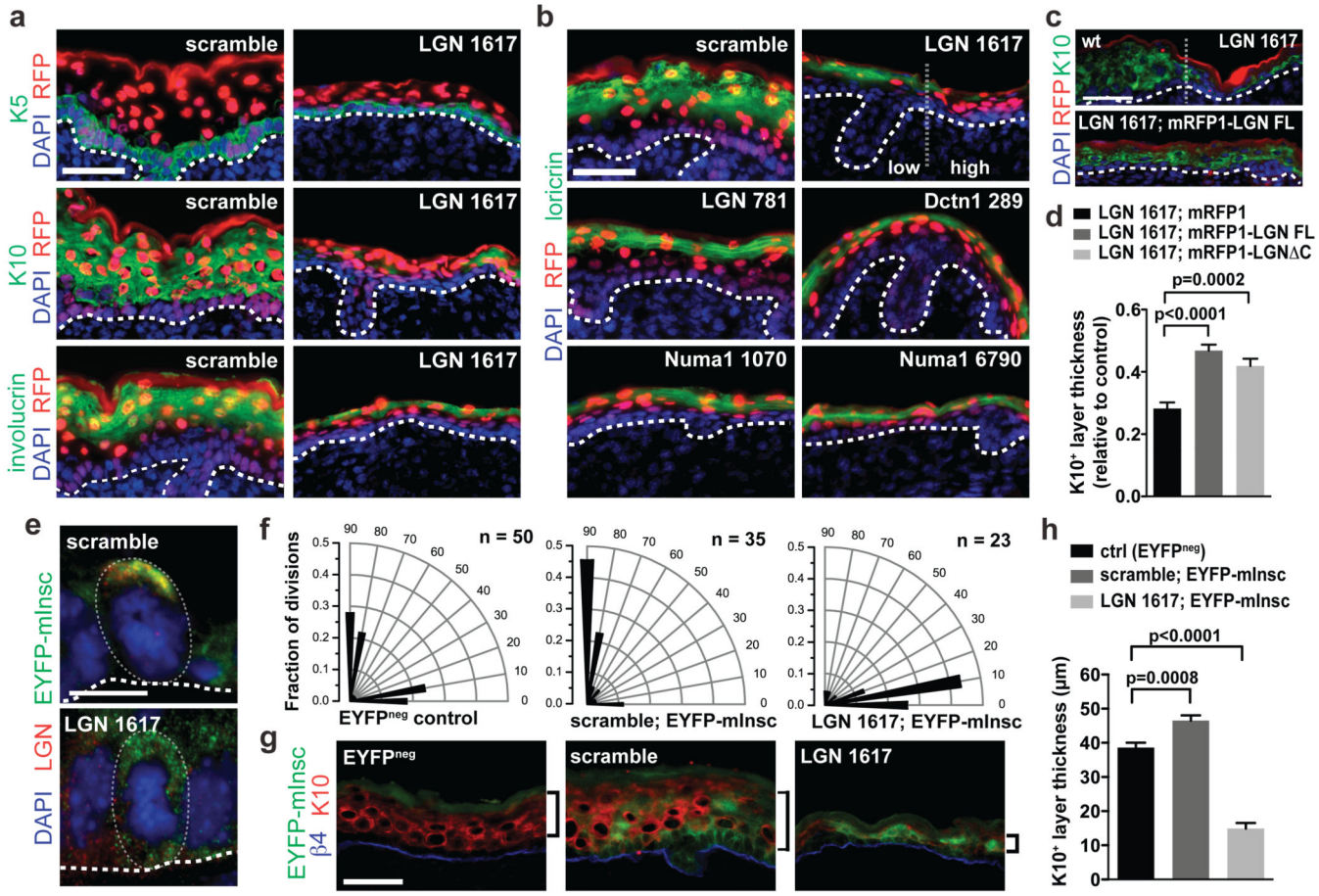

Figure 3. Differentiation defects following *LGN*, *Numa1*, and *Dctn1* depletion

a,b, Reduced terminal differentiation in E17.5 ACD knockdowns. Basally-transduced regions are identified by H2B-mRFP1, always most intense in suprabasal progeny. Note correlation of repressed differentiation with transduction (RFP^+; line demarcates low/high infection boundary). **c,d,** Partial restoration of *shLGN-1617* epidermal defects upon transducing full-length(FL)*LGN* or *LGNΔC* (n>15 fields; n>6 embryos/condition). **e–h,** *EYFP-mInsc* enhancement of LGN-dependent ACDs. **e,** EYFP-mInsc and LGN immunolocalisation in mitotic cells of E17.5 *shScramble* or *shLGN-1617* epidermis after *EYFP-mInsc*. co-transduction. **f,** Quantifications of division axes (n's indicated). (**g,h**) LGN-dependent enhancement of spinous-layer thickness upon mInsc overexpression (n>10 fields; n>3 embryos/condition). Scale bars: 50 μm (**a–c**, **g**), 10 μm (**e**). Error bars are S.E.M.

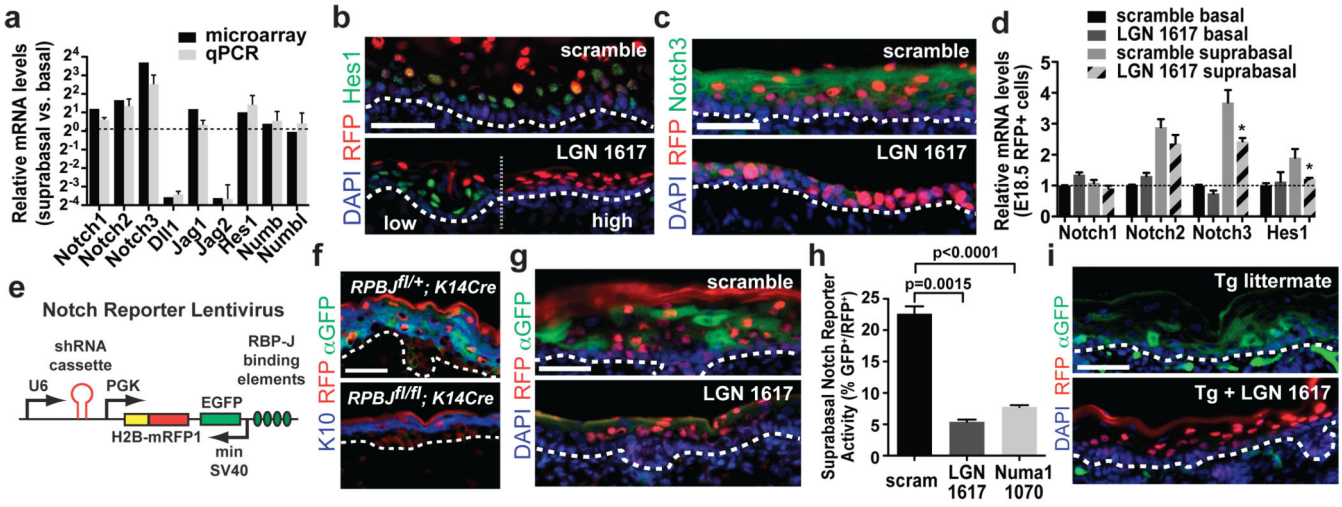

Figure 4. Loss of *LGN* or *Numa1* impairs suprabasal Notch activation

a, qPCR vs. microarray comparisons of Notch pathway gene expression in E14–E15 wild-type epidermis. **b,c,** Diminished Hes1 and full-length Notch3 in *shLGN-1617*-transduced epidermis. Line **(b)** demarcates low/high-infection boundary. **d,** Decreased *Notch3* (p=0.0133) and *Hes1* (p=0.0169) mRNAs in E18 *shLGN-1617* suprabasal cells. Note also dampened suprabasal:basal *Notch1* (p=0.20), *Notch2* (p=0.19). **e,** Lentiviral Notch reporter for coordinate shRNA-knockdown. **f,g** Abrogation of Notch reporter expression ($EGFP^+$), concomitant with differentiation defects, in E17.5 *RBPJ* cKO and *shLGN-1617* epidermis. **h,** Effects of *LGN/Numa1* knockdown on Notch reporter activity (n>24 fields; >3 embryos/condition). **i**, Reduced activity in P0 Notch reporter transgenics transduced with *shLGN-1617;H2B-mRFP1*. Error bars in **a,d** represent S.D; S.E.M. in **h**. Scale bars: 50μm. For qPCR (**a,d**), n's are triplicates from 2 separate experiments.

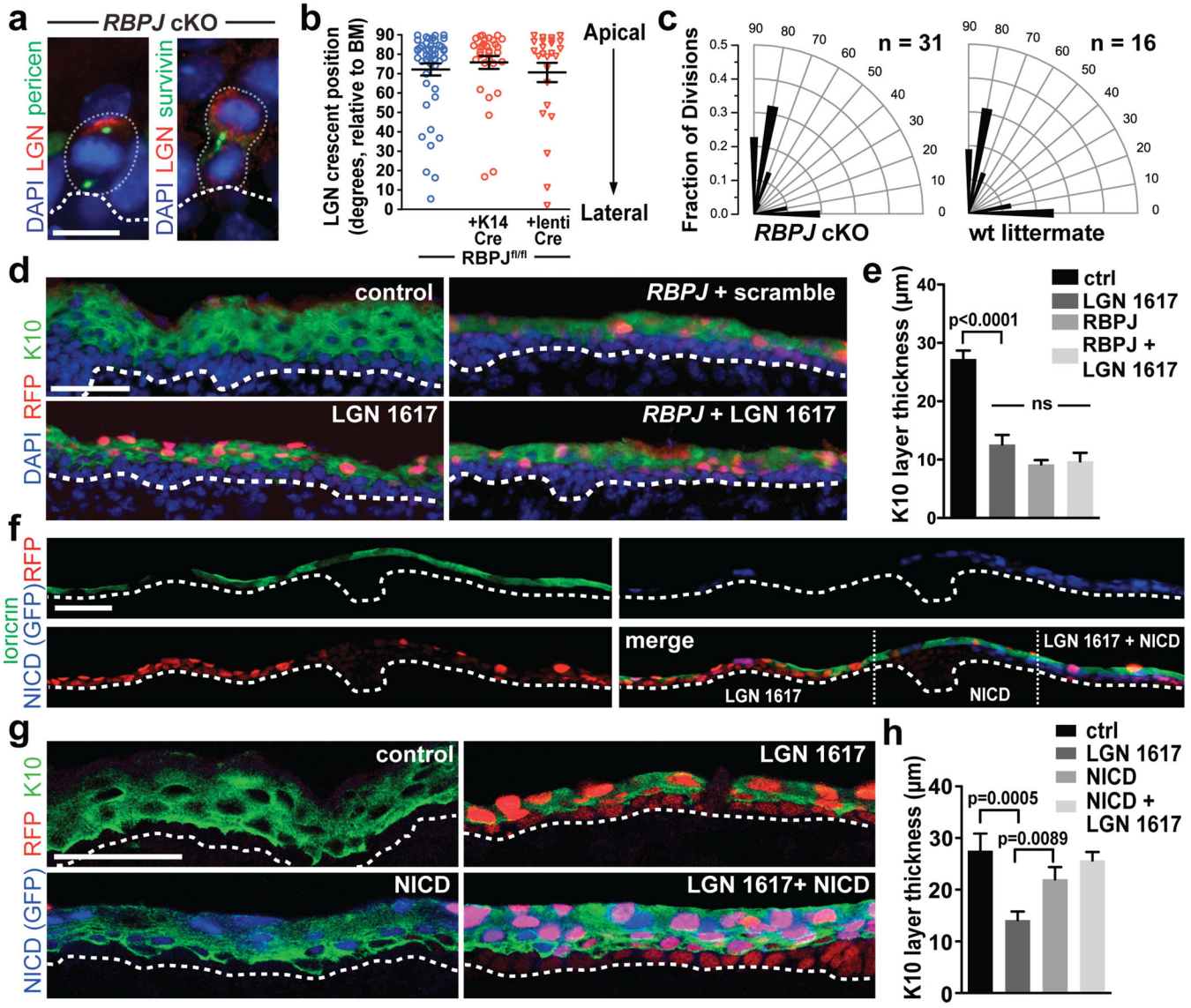

Figure 5. Genetic interaction between ACD and Notch pathways

a–c, Normal LGN localization and ACDs in *RBPJ* mutants (each dot represents one data point in **b**, n's indicated in **c**). **d**,**e,** Analyses of differentiation defects in E17.5 headskins from control or *RBPJ*$^{fl/fl}$ embryos transduced at E9.5 with *shLGN-1617;H2B-mRFP1* (LGN1617), *shScramble;NLS-Cre-mRFP1* (*RBPJ*+scramble), or *shLGN-1617;NLS-Cre-mRFP1* (*RBPJ*+LGN1617). Comparable defects in double and single mutants/knockdowns, suggest a common pathway for *RBPJ* and *LGN*. **f–h,** Restoring Notch signalling rescues *shLGN-1617* differentiation defects. Headskin (**f**); backskin (**g**,**h**). Combinations of single and double mutant clones (separated by vertical lines) expressing *shLGN-1617* (red) and active NICD (GFP, pseudocolored in blue) were generated by co-infecting E9.5 *Rosa-Lox-stop-Lox-NICD-IRES-GFP*-knockin embryos with *shScramble/shLGN-1617;H2B-mRFP1* and *NLS-Cre*. Scale bars: 10μm (**a**); 50μm (**d, f, g**). Error bars represent S.D. (**b**), S.E.M.

(**e**,**h**). p values from two-tailed student's t-tests are indicated; ns: not statistically significant. For **e**,**h**, n>10 fields; n>3 embryos.